Luomaniemi, Rasmus; Lehtovuori, Anu; Ilvonen, Janne; Khripkov, Alexander; Viikari, Ville

Extremely Low-Profile Tunable Multiport Handset Antenna

Published in:
IEEE Transactions on Antennas and Propagation

DOI:
10.1109/TAP.2021.3111320

Published: 01/02/2022

Document Version
Publisher's PDF, also known as Version of record

Extremely Low-Profile Tunable Multiport Handset Antenna

Rasmus Luomaniemi, *Graduate Student Member, IEEE*, Anu Lehtovuori, Janne Ilvonen, Alexander Khripkov, *Member, IEEE*, and Ville Viikari, *Senior Member, IEEE*

***Abstract*— This article presents an extremely low-profile tunable antenna design for smartphones with height of only 0.75 mm. The proposed antenna is integrated into the back cover of the device to utilize the existing gap between the battery and the back cover as efficiently as possible. By utilizing both tunable components and adjustable feeding weights, the designed multiport antenna system covers 3300–4200 MHz frequency range with 100 MHz instantaneous bands. In addition to just frequency tuning, these tunable elements can be utilized to adapt the antenna for different operation environments, such as changes in the structure of the device or the user effect. We show that the proposed antenna can be extended for two- and four-element multiple-input multiple-output (MIMO) operation. The proposed design is manufactured and measured, and the results confirm good antenna performance with average total efficiencies of 35% and 25% in free space and with a hand phantom, respectively.**

***Index Terms*— Antennas, low-profile antennas, multiport antennas, reconfigurable antennas, tunable antennas.**

I. Introduction

MOBILE antenna designers are facing major challenges in reaching the increasingly difficult goals set by both new mobile communication system standards as well as current trends in esthetic design of the device. Although the millimeter-wave frequencies, e.g., in the 20–30 GHz band, have attracted a lot of attention lately, the lower sub-6 GHz frequencies continue to have an important role in the current and future smartphones due to the good compromise between the coverage area and the high data rates that they offer [1]. As the 700–960 MHz low band and the 1700–2700 MHz middle-high band antennas normally occupy the metal rim of the device [2]–[6], the space available for additional 3500 MHz antennas is very limited. Although a large number of designs for 4, 8, 10, or even higher order multiple-input multiple-output (MIMO) systems have been published lately [7]–[15], combining all the antennas into a realistic device model is very challenging due to the total volume required and the challenges in integrating all of the antennas with the metal rim.

Since the metal rim is already fully occupied, new types of antennas placed elsewhere in the device are needed. One of the most attractive options is the back cover area and especially the region on top of the battery. However, the volume is extremely limited with height less than 1 mm so very low-profile antennas which can be integrated into the device are needed.

Different types of low-profile antennas have been published, e.g., in [16]–[24]. Even these antennas have several weaknesses that make them unsuitable for the purpose. The impedance surfaces used by many designs require the utilization of the entire area of the device which makes it difficult to integrate with other components, such as the cameras. Although many of these designs have been considered as low-profile antennas, their sizes are still too large for the modern smartphones where only places with heights less than 1 mm are available. Also, the operation bands often do not cover the whole 3300–4200 MHz band.

Decreasing the height of the antenna inevitably increases the Q-factor and as a consequence, either the achievable efficiency level or the bandwidth is reduced [25], [26]. One way to improve the performance while making the antenna smaller is to introduce tunable components in the matching networks or as aperture matching components to cover only part of the band instantaneously. Traditional tuning methods include tunable capacitors or varactor diodes: [27]–[29], switches and PIN diodes [3], [30], [31], and switches connected to fixed inductors and capacitors [32]–[34]. In addition to these, the frequency tuning can also be realized with multiport antennas using the injection matching technique [35], [36] or the antenna cluster technique [37], [38].

In this work, we design an extremely low-profile antenna that uses both tunable matching components and multiport feeding arrangement utilizing tunable feeding weights. A main radiator is built on top of the battery in the back cover and non-contacting elements are used for excitation. Thus, the effective height of the antenna can be increased, and the existing volume is utilized more efficiently than with traditional solutions. Two exciter elements can excite new resonances compared to using only a single feed making it possible to cover the whole 3300–4200 MHz band with 100 MHz instantaneous bandwidth. The tunable elements make it possible to adapt the antenna operation to changing operation environment, such as changes in the battery height and the user effect. The proposed

Manuscript received February 1, 2021; revised July 2, 2021; accepted August 8, 2021. Date of publication September 15, 2021; date of current version February 3, 2022. This work was supported by Huawei Technologies Finland. The work of Rasmus Luomaniemi was supported in part by the Aalto University School of Electrical Engineering Doctoral School, in part by the Nokia Foundation, in part by the HPY Research Foundation, and in part by the Finnish Foundation for Technology Promotion. *(Corresponding author: Rasmus Luomaniemi.)*

Rasmus Luomaniemi, Anu Lehtovuori, and Ville Viikari are with the Department of Electronics and Nanoengineering, Aalto University, Espoo, 00076 Aalto, Finland (e-mail: rasmus.luomaniemi@aalto.fi).

Janne Ilvonen and Alexander Khripkov are with Huawei Technologies Finland, 00180 Helsinki, Finland.

Color versions of one or more figures in this article are available at https://doi.org/10.1109/TAP.2021.3111320.

Digital Object Identifier 10.1109/TAP.2021.3111320

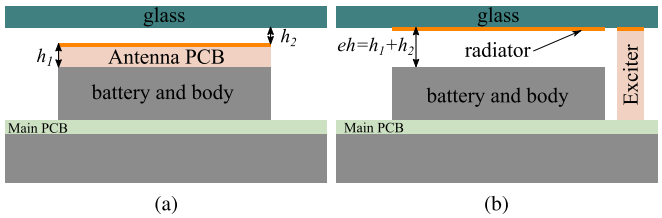

Fig. 1. (a) Traditional patch antenna and (b) concept of the proposed antenna.

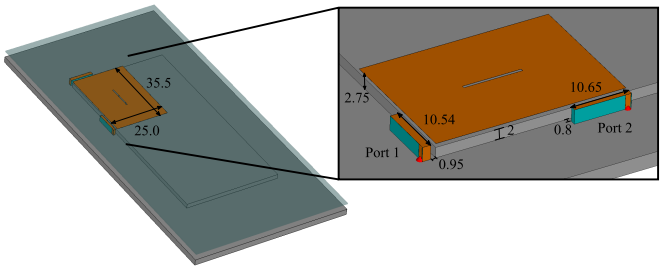

Fig. 2. Simplified model of the proposed multifeed antenna. All dimensions in mm.

antenna design and its operation are experimentally verified with results showing good performance.

II. Operation Principle of the Proposed Antenna

A. Prestudy of the Antenna Structure

Fig. 1 shows the side views of a traditional patch-type antenna on top of a battery and the new concept of the proposed antenna structure integrated into the glass back cover. Due to manufacturing tolerances and to enable the expansion of the battery without braking any of the other components or structures, there has to be a gap between the battery/antenna and the bottom of the back cover. By integrating the main radiator into the back cover and exciting it with noncontacting elements from the outside, we can increase the effective height of the antenna. If we assume that the traditional patch has a height of $h_1 = 0.5$ mm and a gap of $h_2 = 0.25$ mm is required, the proposed antenna can have an effective height of $eh = h_1 + h_2 = 0.75$ mm in the same structure. Given this extremely small antenna height, even small differences can have large effect on the efficiency. The 0.25 mm increase for the 0.5 mm height increases the antenna volume by 50% meaning significant improvements in the antenna performance. In addition, the exciter elements with their feeding structures and matching circuits can be placed on the same main printed circuit board (PCB) with the components of other systems in the device without the need for any additional PCBs just for the antennas.

Fig. 2 shows a simulation model of the antenna where the device body and battery are modeled with aluminum and the back cover with glass ($\epsilon_r = 6$). The antenna and the exciter elements are modeled with copper with conductivity $\sigma = 5.8 \times 10^6$ S/m used for realistic representation of losses. The exciter elements use Preperm PPE260 RF-plastic as supporting structures. The exciter elements are inverted-F antennas (IFAs) with the grounding strip and the feeding line

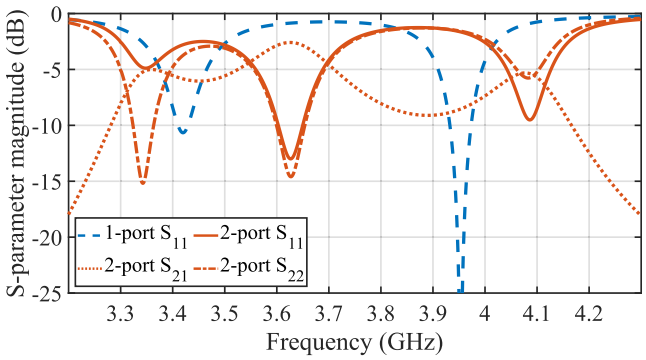

Fig. 3. Scattering parameters for one-port and two-port antennas.

placed close to each other at the end of the element. The characteristic mode analysis shows that the main radiator with dimensions of 35.5×25.0 mm^2 has only one mode, with currents mainly along the longer dimension of the radiator, in resonance in the 3300–4200 MHz frequency range. Therefore, the exciter elements are initially placed to excite this mode with currents mainly along the longer dimension of the radiator.

Scattering parameters for the two-port structure of Fig. 2 and the same structure with only one exciter element are shown in Fig. 3. Using two feeds, an additional resonance is excited between the two resonances of the single feed case. We can also notice that the coupling between the ports is relatively high, from -9 to about -3 dB, but that can be beneficial when the antenna cluster technique is used as will be explained later in Section II-B.

To study the generated resonances and the effect of the size of the slot in the main radiator, Fig. 4 shows the surface currents for three different dual feed structures and also for the single-feed case for comparison. The corresponding S-parameters are presented in Fig. 5. First, these results demonstrate the benefits of the two feeds. With a single feed, the currents are mainly along the longer edges of the patch in the whole frequency band. When the second feed is introduced, a new resonance with a diagonal current distribution is excited as a result of the interaction between the two feeds. With this new resonance, the required frequency band can be covered more efficiently, demonstrating one of the benefits of multiport antennas in this case. Second, the slot can be used to tune the frequencies of these resonances by affecting them differently depending on the dimensions of the slot. As Fig. 5 shows, when the length of the slot is increased, only the middle resonance is shifted lower in frequency while the first and third are practically unaffected. This is due to the slot length making the diagonal current path longer while the path along the long edges is not changed. Making the slot wider, on the other hand, lowers the first and third resonance frequencies while having no effect on the second resonance. Wider slot increases the length of the current path along the edges of the patch while the diagonal currents are not significantly changed.

B. Study of the Tunable Operation

To utilize the multiple feeds as an antenna cluster, we shortly introduce the required theory here. The key element

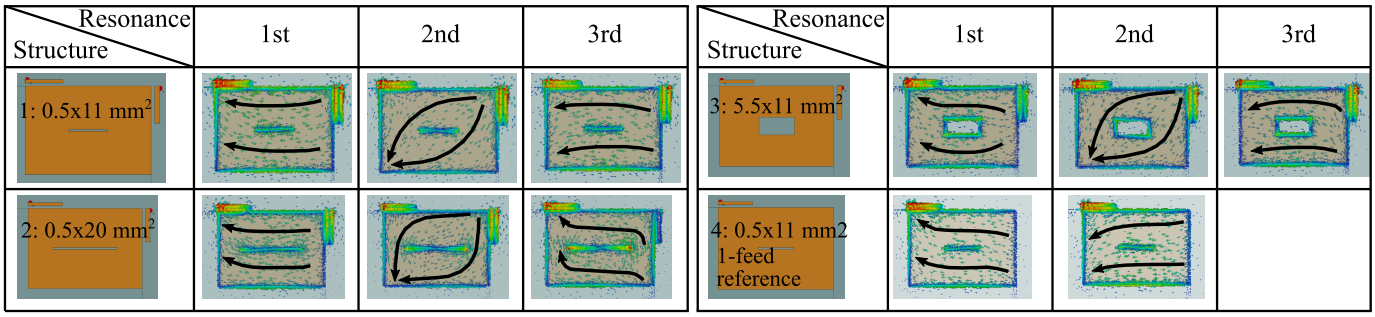

Fig. 4. Surface currents for dual-feed antennas at different resonances with three different slot sizes and a single-feed reference antenna.

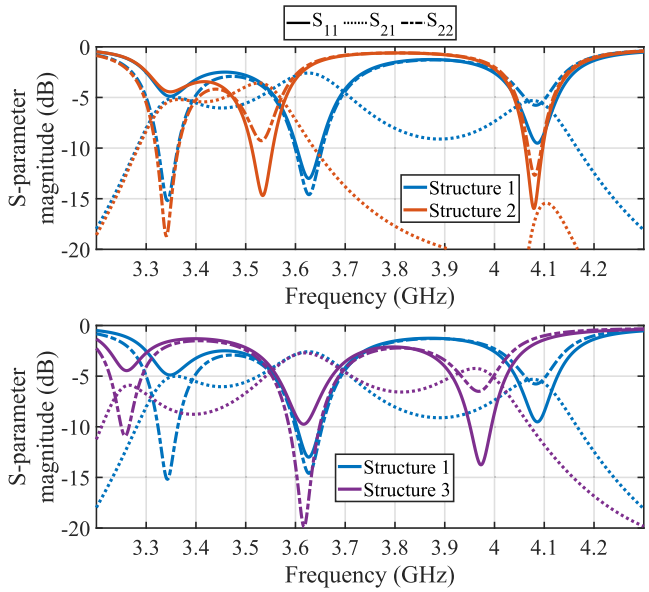

Fig. 5. Scattering parameters for different length of the slot (top) and different width of the slot (bottom).

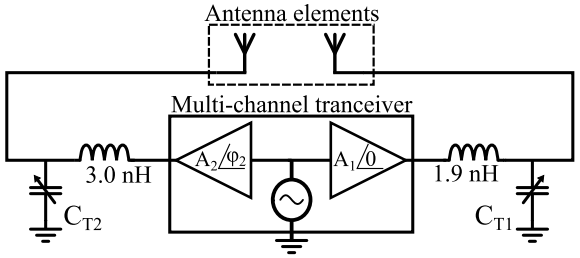

Fig. 6. Tunable matching circuit topology for the simplified two-port antenna cluster.

in utilizing multiple feeds is to properly choose the amplitudes and phases of the feeding signals [37]. With proper feeding arrangement, the reflected signals partly cancel each other leading to increased radiated power and higher efficiency. Optimal feeding weights for a certain antenna structure are obtained as the magnitudes and phases of the complex eigenvector corresponding to the largest eigenvalue of the radiation matrix (calculated either from the scattering parameters or the far-field patterns). For more details, see [38] and [39].

To be able to utilize the multiple actively fed ports for an efficient antenna cluster, a proper level of coupling between the ports is required [40]. Because of this, the relatively high coupling seen in Fig. 3 is not actually detrimental to the operation of the antennas, but it can rather be beneficial. The optimal amplitude and phase for each feed depends on the frequency and by changing these weights, frequency tuning can be achieved across wide frequency bands. In realistic usage, the feeding weights cannot be freely modified for arbitrary frequencies since the operation has to be fixed for a certain bandwidth determined by communication system requirements. Therefore, in this work, the weights are set constant for 100 MHz bands to cover the whole 3300–4200 MHz range.

The matching network components are optimized numerically simultaneously with the complex feeding weights to obtain be the optimal performance available from the multiport system. To take into account both the losses of the materials and the matching network components, the antenna performance is calculated from the far-field patterns of the elements and total efficiency is used as the optimization goal on every step of the process.

With the matching network designs for antenna clusters, it is important to take the feeding weights into account in the design process. This is done by combining both the matching component and the feeding signal optimization into the same process. In this work, we use a numerical optimization method similar to one presented in [41] to find both the fixed components and the values for the tunable capacitors when also the optimal feeding amplitudes and phases are taken into account.

Fig. 6 shows the schematic of the tunable elements with the two-port antenna. The tunable matching circuits consist of one fixed inductor and a tunable capacitor for each feed. At this point, we model the tunable capacitors with an ideal capacitor and the losses with a resistor whose value depends on the Q-factor of the component. As values for these, we use the capacitance in the range of $C_T \in [0.6,\ 3.2]$ pF and $Q \in [20,\ 10]$, which are similar to real components available in this frequency range.

The amplitudes and phases of the feeding signals and the tunable capacitor values are shown in Fig. 7 and the resulting S-parameters in Fig. 8. Instead of the S-parameters, the multifeed operation is better described with total active reflection coefficient (TARC) [42], corresponding to the reflection coefficient of traditional single-feed antennas. TARC for ideal capacitors and total efficiency for both ideal and lossy

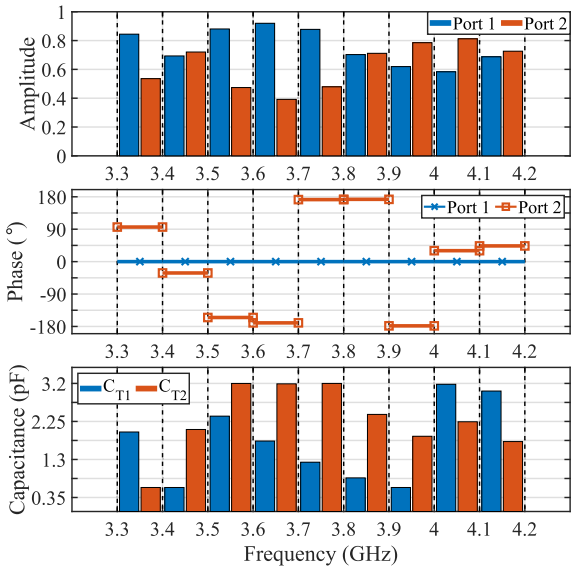

Fig. 7. Tunable elements for the simplified two-port antenna cluster.

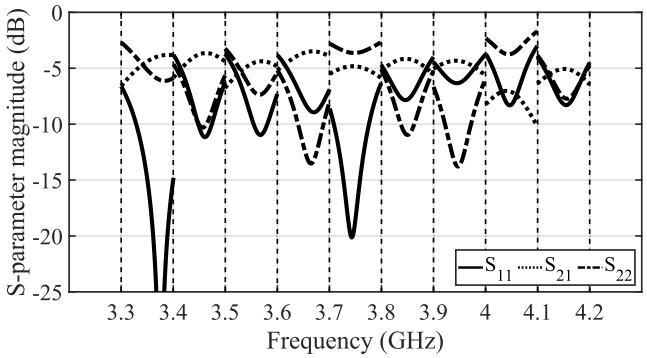

Fig. 8. S-parameters of the simplified two-port antenna cluster tuned for 100 MHz subbands from 3.3 to 4.2 GHz.

tunable capacitors are shown in Fig. 9. The results show that using two feeds and the tunable elements, the three resonances of the antenna structure can be used to cover the whole band with 100 MHz instantaneous bandwidth. TARC is better than -7 dB in the whole band and total efficiency with ideal capacitors is better than 40%. The more realistic lossy capacitors have only a small effect in the efficiency and better than 35% total efficiency is achieved even in this case, demonstrating that the proposed method is not too sensitive for losses of the matching networks.

C. Study of Adaptivity for Changes in the Structure

As the antenna structure is placed above the battery, changes in the structure can affect the antenna operation. The most probable change is small increase in the battery height, e.g., due to swelling. Since this effectively decreases the distance between the main radiator and the antenna ground, it is likely to affect to the antenna performance and decrease performance. However, as we have now several tunable elements in the design, these can be used to compensate these changes and adapt the operation for changing environment.

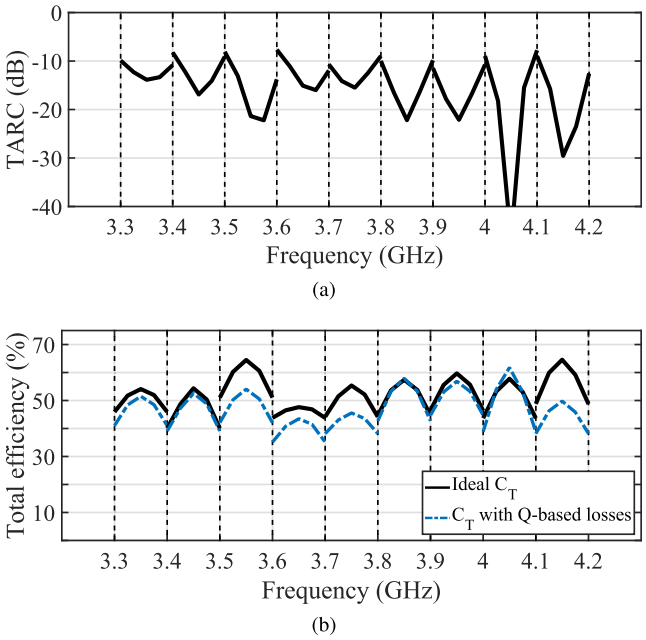

Fig. 9. (a) TARC and (b) total efficiencies with ideal tunable capacitors and capacitors with Q value based losses.

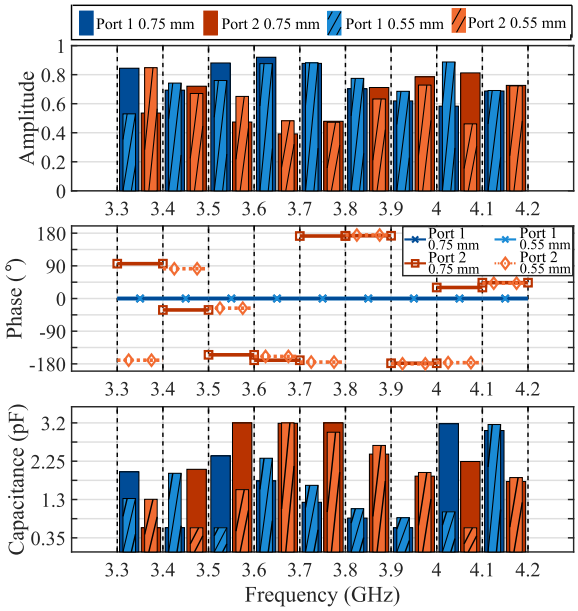

Fig. 10. Tunable elements for two different battery heights.

To study the effect of different battery heights, total efficiencies are compared for two different values of the gap between the top of the battery and the main radiator: the original 0.75 mm and a smaller 0.55 mm. For the smaller gap, the feeding weights and the tunable capacitor values are reoptimized with the new values presented in Fig. 10 along with the original ones for comparison. The results in Fig. 11 clearly show that the tunability can be used to compensate the degradation in efficiency due to changes in the structure.

With the original tunable elements, the minimum efficiency drops down to 16% because the resonances shift to

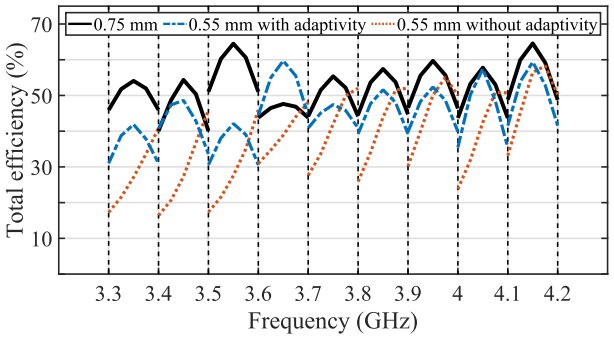

Fig. 11. Effect of changes in battery height on total efficiency and its compensation with reoptimization of the tunable elements.

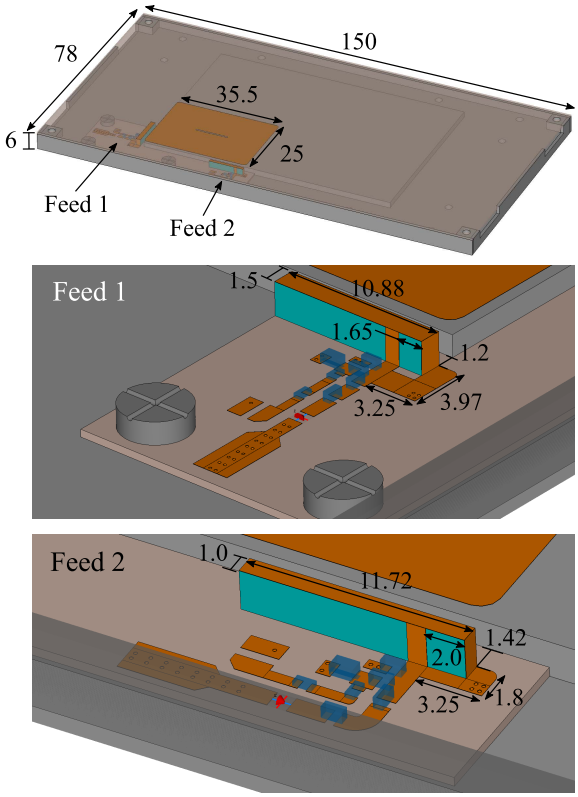

Fig. 12. Final antenna structure and close-ups of the IFA-type exciter elements. All dimensions in mm.

higher frequencies. With the reoptimized tunable elements, especially the tunable capacitors, the frequency shifts can be compensated, and better than 30% efficiency is retained. Because changes in the battery height can be assumed to be relatively slow in normal usage, this adaptivity could be realized, e.g., by monitoring received power levels and adjusting the values of the tunable elements accordingly to calibrate the antenna if needed. More detailed realization of this is out of the scope of this article.

III. Full Antenna Structure and Simulation Results

A. Final Antenna Structure

Based on the results from Section II, the proposed multiport antenna concept is elaborated into a full realizable antenna design. First, for easier manufacturability of antenna prototypes in later stages, the back cover is made from Rogers RO3006 substrate which has permittivity $\varepsilon_r = 6.5$ close to that of glass materials used in real devices. This material is used so that the main radiator in the back cover can be manufactured with standard PCB processes.

The final antenna structure and both of the feeding elements with detailed dimensions are shown in Fig. 12. Some modifications compared to the simplified model of Section II are required to guarantee reliable manufacturing of the prototype. Note especially the short circuiting strips between the feeding lines and the grounding pads of the IFA-type exciter elements, as shown in Fig. 12. Addition of these strips makes it possible to increase the distance between the feeding lines and the grounding pads without affecting the operation, thus improving the manufacturing tolerance of the design.

Next, PCB for the antenna elements and matching networks are designed. Rogers RO4350B substrate material is used for this PCB. Matching networks with three fixed elements and one tunable element for each feed are used. To realize the tunable capacitors, varactor diodes are chosen because the physical components and simulation models are widely available, and they can be controlled with dc-voltages without the need for any additional digital circuitry. To realize the exciter elements, the copper patterns are manufactured on a flexible PCB made from 25 μm thick DuPont material which is then glued to the supporting plastic structure. These elements are then attached to the main PCB by soldering the feeding and grounding strips to the corresponding pads.

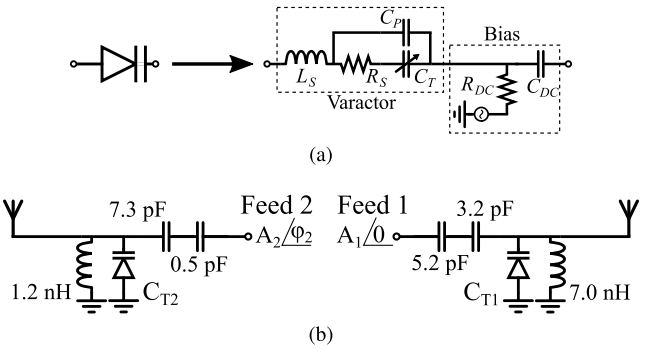

Fig. 13. (a) Varactor diode circuit model and (b) tunable matching circuits for the full antenna structure.

B. Single Antenna Results

The used circuit model for the varactor diode is shown in Fig. 13(a). The diode finally chosen for the design is Skyworks SMV2020-079LF with the following parameters: $L_S = 0.7$ nH, $R_S = 2.5\ \Omega$, and $C_P = 0$ pF. The capacitance C_T can be tuned from 0.35 to 3.20 pF. The S-parameters of the antenna structure without any matching components are shown in Fig. 14(a). Fig. 14(b) shows the tuned S-parameters when the matching networks of Fig. 13(b) are applied. The results show that before applying the tunable matching, both ports have three resonances similar to the simplified model studied in Section II. With the matching networks, these resonances can be tuned to cover the whole 3.3–4.2 GHz band with

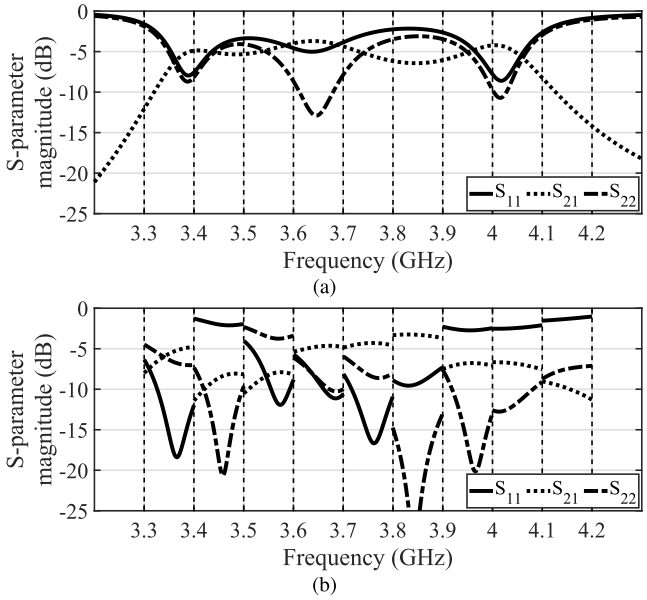

Fig. 14. Simulated S-parameters (a) without matching components and (b) with tunable matching networks for the full antenna strucutre.

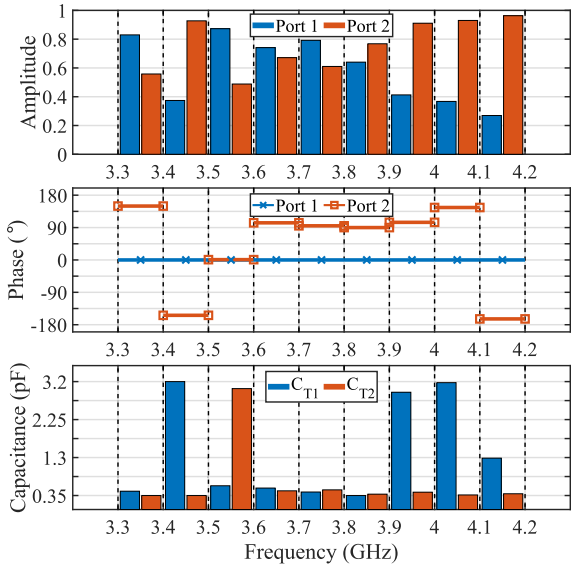

Fig. 15. Tunable elements for the full antenna structure.

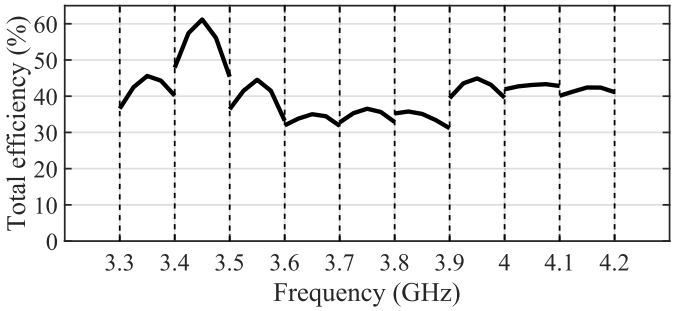

Fig. 16. Simulated total efficiencies for the full antenna structure.

100 MHz instantaneous bandwidths as the tuned S-parameters show.

The feeding amplitudes and phases and the optimized tunable capacitances are shown in Fig. 15. These results demonstrate the benefits of the cluster technique. For example, the feeding amplitudes and the tuned S-parameters show that

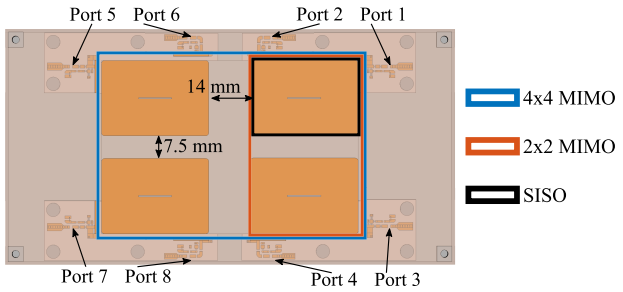

Fig. 17. Examples of the possible MIMO configurations of the proposed antenna design.

in addition to choosing optimal phase difference, also the power balance between the two feeds can be tuned so that the resulting efficiency is maximized. Fig. 16 shows the corresponding simulated total efficiencies. Better than 30% efficiency is achieved on the whole band confirming that the proposed method and antenna design can be used to realize antennas with good performance in the extremely small volume available for antennas between the back cover and the battery.

C. MIMO Operation

The proposed antenna design can be extended to enable MIMO operation. Depending on the wanted MIMO configuration and space available, two-element or even four-element MIMO system can be realized. Fig. 17 shows the MIMO antenna structures studied in this article. For the 2×2 results, only the two antennas (ports 1–4) are included in the simulation model and 4×4 results have the full structure. To evaluate the MIMO performance, we calculate the ergodic capacity from the simulated far-field patterns using the method presented in [43].

Fig. 18 shows the coupling parameters between all the eight ports for the four-element configuration with the tunable matching networks applied. Because the radiation modes (Fig. 4) have strong currents primarily on the main radiator in the back cover, the coupling between different MIMO antennas is low. The results show that coupling is from -80 to -20 dB thus sufficing for MIMO operation. The envelope correlation coefficients (ECCs), calculated from the far-field patterns, are presented in Fig. 19. The ECCs are mainly below 0.05 and always below 0.15 meaning that the effect of the correlation on the MIMO performance is small [43]. Finally, Fig. 20 shows the single-input single-output (SISO), 2×2 MIMO, and 4×4 MIMO capacities. For comparison, also the ideal maximum capacities for each case are shown. These results confirm that good MIMO performance is achieved. All three of the studied cases achieve about 78% of the corresponding ideal capacity.

D. User Effect

The user effect, i.e., how the antenna performance is changed in the presence of the user, can have a large impact on the antenna's operation. To study this, the antenna performance is simulated with a hand phantom as shown in Fig. 21 using the two-element MIMO antenna configuration. The hand is

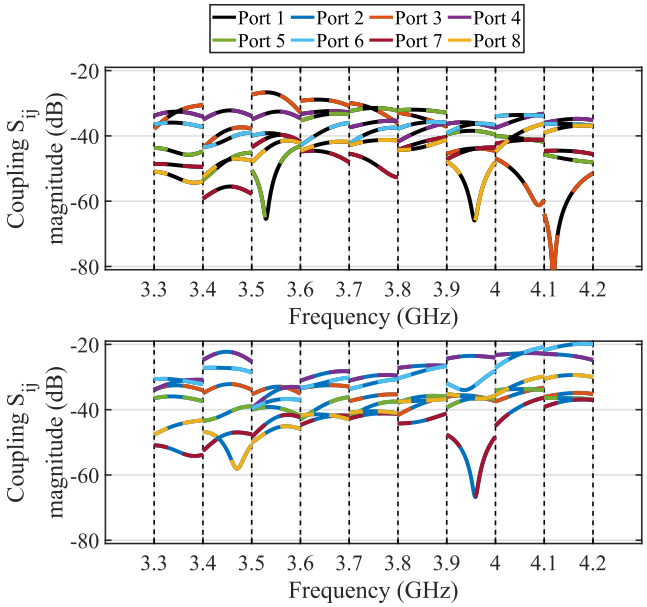

Fig. 18. Coupling parameters for the four-element MIMO configuration.

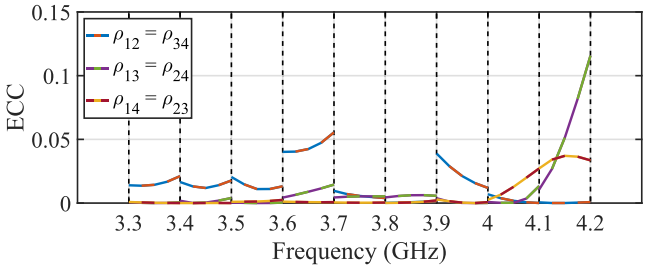

Fig. 19. ECCs for the four-element MIMO configuration.

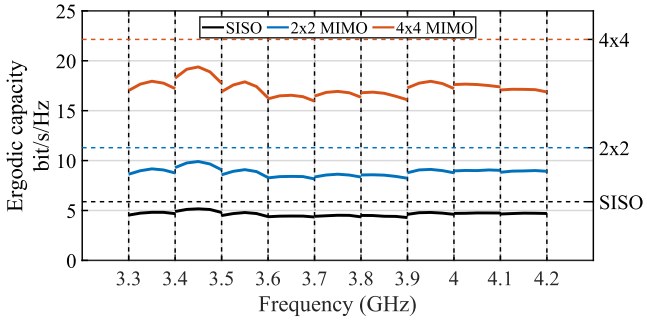

Fig. 20. Capacities for SISO and different MIMO configurations.

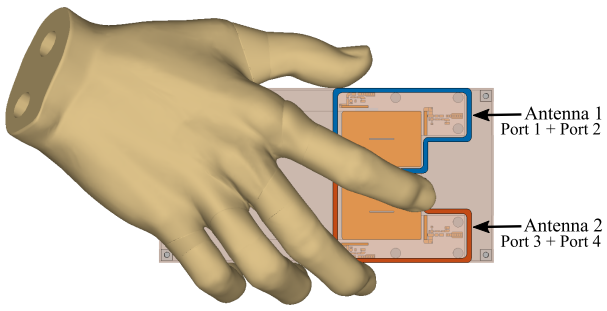

Fig. 21. Simulation model for the user holding the device.

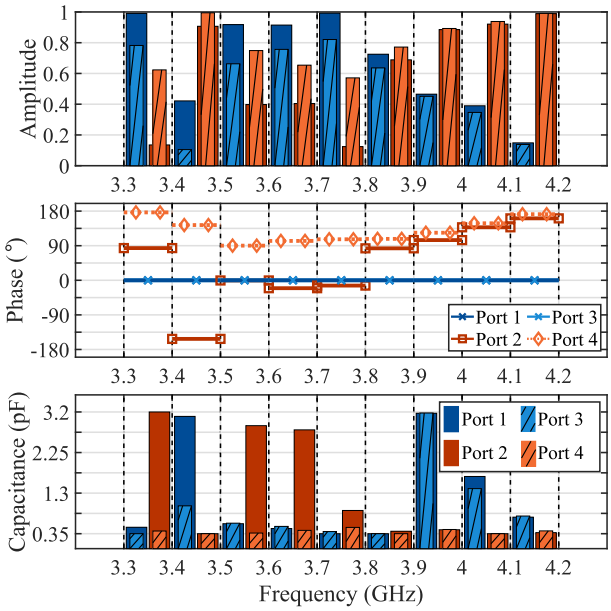

Fig. 22. Tunable elements reoptimized for the user effect.

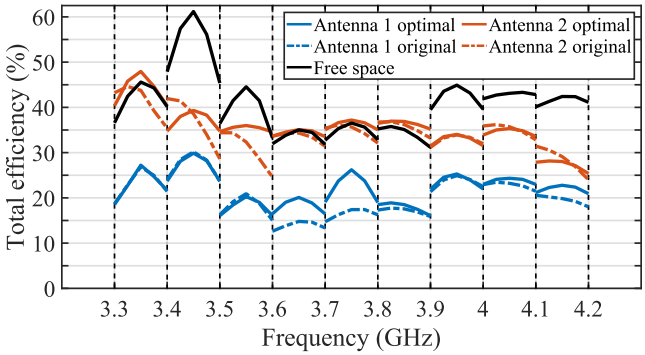

Fig. 23. Simulated total efficiencies with the user's hand.

holding the device so that the index finger is placed on the back cover roughly on top of the antenna main radiators on the bottom side.

An important factor with the antenna clusters and the user effect is the way how the feeding signals and their reconfigurability is used. By properly adapting the feeding signals for the changing environment, it is possible to reduce the user effect [44]. In this work, in addition to the feeding signals, also the tunable capacitor values are reconfigured to the case where the user's hand is holding the device. Therefore, two different results for both of the antennas in Fig. 21 are simulated. First, the same tunable elements as in free-space conditions (Fig. 15) are applied, and second, the tunable elements are reoptimized to give maximum total efficiency with the user.

Figs. 22 and 23 show the user-optimal tunable elements and the corresponding simulated total efficiencies both with the optimal as well as the original tunable elements. The reoptimization of the tunable elements improves the efficiency on some frequency bands and the reoptimized tunable elements clearly differ for the two antennas. The largest improvements

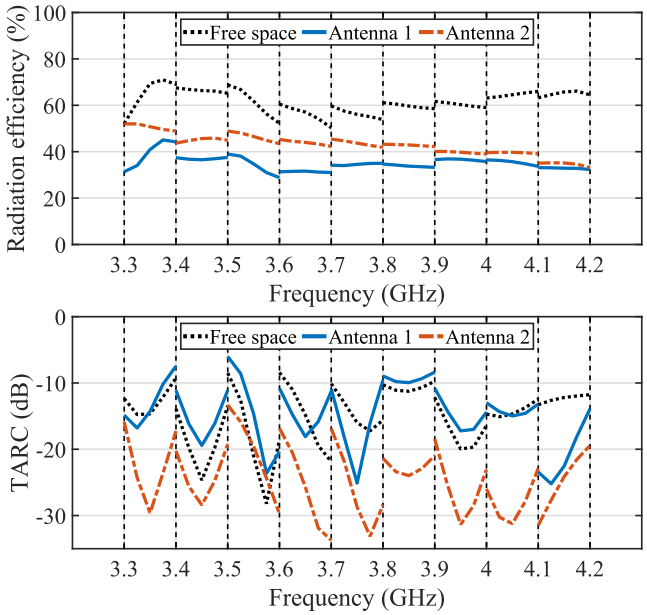

Fig. 24. Radiation efficiencies and TARCs with the user and in free space.

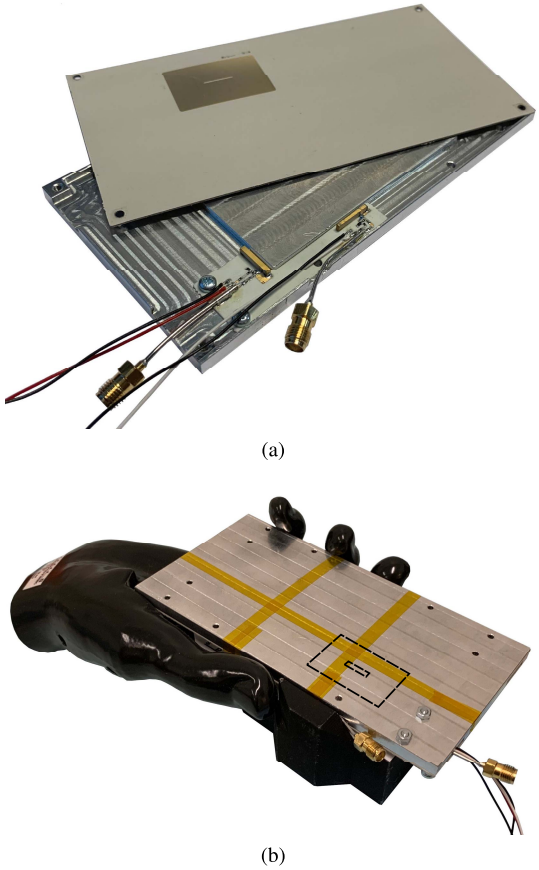

(a)

(b)

Fig. 25. (a) Prototype with the back cover removed. (b) Hand phantom used in the measurements and the location of the antenna shown with dashed line.

for antennas 1 and 2 are about 50% and 40%, respectively, compared to operation with the free-space tunable elements. Even without the reoptimization, both of the antennas have reasonable performance.

The effect of the user is clearly different for the two antennas. Antenna 1 achieves an average efficiency of 22% while antenna 2 has an average efficiency of 35%. This difference can be studied using the radiation efficiencies and TARCs shown in Fig. 24. The results show that there is smaller difference in the radiation efficiencies of antennas 1 and 2 than there is in TARCs. This suggests that the difference in total efficiency is more due to deteriorated impedance matching than degraded radiation efficiency. As the large Q-factor is known to be a limiting factor for the operation of antennas with small height [25], [26], the presence of the lossy material of the user's hand can actually be beneficial by lowering the Q-factor. Antenna 1 has similar TARC with the user as in free space, leading to lower total efficiency due to lower radiation efficiency. Antenna 2, on the other hand, has better TARC with the user than in free space, and can therefore achieve better total efficiency than antenna 1. Despite the lower radiation efficiency, almost equal performance compared to free-space operation in many frequency bands is achieved due to the improved matching.

Naturally, the previous results apply directly only to the studied case with the standardized hand model used. In real use, every user can hold the device differently, and, for example, the location of the fingers with respect to the antennas under the back cover could vary. However, the studied case with two differently placed antennas demonstrates well the differences that can be expected from various hand gestures. The user's hand causes more significant changes in the matching levels and less changes in radiation efficiency. Reasonable performance can be expected, especially with MIMO configurations, for different hand grips.

IV. Prototype and Measurement Results

A prototype of the proposed antenna is manufactured and measured. As explained in Section III-A, the back cover is made from a PCB material with similar electrical properties as glass that would be used in real products The prototype with open back cover is shown in Fig. 25(a) and with the hand phantom in Fig. 25(b). The measurement process is as follows. First, the initial values for the varactor diode control voltages are found based on measured S-parameters. Next, the far-field patterns of both feeds are measured individually while the other is terminated with 50 Ω load. Then the optimal feeding amplitudes and phase are calculated from the far-field patterns and the total efficiency is calculated numerically. When required, this process is repeated to fine-tune the antenna to operate with maximum efficiency over each subband. Similar to the simulated user effect results in Section III-D, the tunable elements are also tuned separately for operation with the hand phantom.

The tunable elements for free-space operation and operation with the hand phantom are presented in Fig. 26 and the efficiencies in free space and with the user in Fig. 27. The differences in the tunable elements, especially the capacitances, for free space and with hand phantom are relatively small. Due to the somewhat cumbersome measurement process including measurement of each far-field pattern several times,

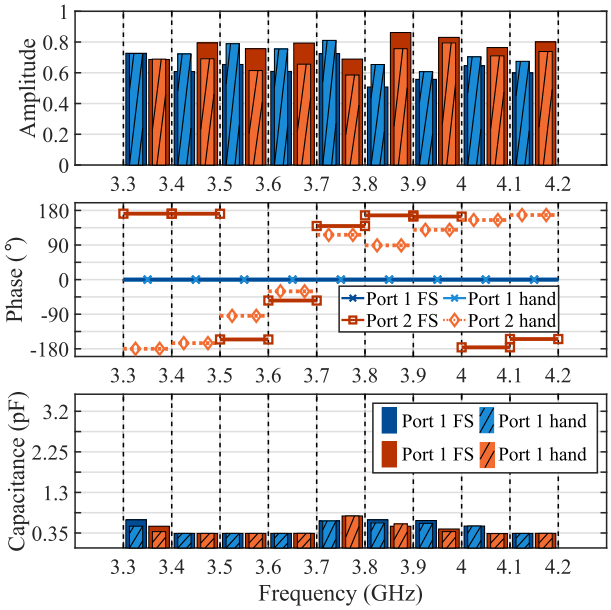

Fig. 26. Tunable elements for the measured prototype in free space and with the hand phantom.

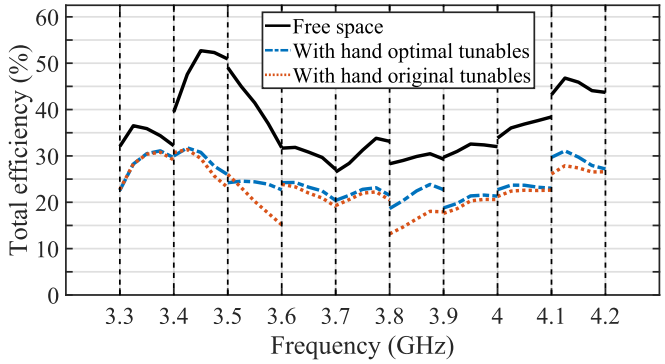

Fig. 27. Measured total efficiencies of the prototype in free space and with the hand phantom.

it is possible that the best settings have not been found. For a more practical way to realize the optimization of the tunable elements for different usage scenarios, a real-time over-the-air (OTA) throughput or received power based measurement setup, such as one presented in [45], could be studied in the future. Fig. 27 shows that the measured efficiencies correspond well with the simulated ones. About 35% total efficiency is achieved on average in free space and about 25% with the hand phantom and optimal tunable elements. With the extremely small height of only 0.75 mm for the antenna in the difficult environment of modern smartphone, these results can be considered very good.

V. Conclusion

This article presented an extremely low-profile antenna design for smartphone applications. The main radiator of the antenna is integrated into the back cover of the device on top of the battery and noncontacting exciter elements are placed on the main PCB. This allows us to effectively utilize the gap between the battery and the back cover for the antenna and increase the effective volume of the antenna compared to traditional designs. Using multifeed techniques, a new resonance is created which enables us to cover the whole 3.3–4.2 GHz band with 100 MHz tunable subbands. The frequency tuning is realized with a combination of tunable matching networks and tunable feeding amplitudes and phases. We showed that the antenna retains good performance also with the user holding the device or in case that swelling of the battery decreases the antenna volume. The proposed design can also be extended to MIMO operation with two or four elements for increased data transfer rates. The measured prototype results confirm that good performance can be achieved despite the difficult design platform, with average efficiencies of 35% in free space and 25% with hand phantom. With the proposed design method, very small volumes and challenging locations inside smartphones can be utilized by future antennas.

Acknowledgment

The authors would like to thank Albert Salmi from the Department of Electronics and Nanoengineering, Aalto University, Espoo, Finland, for his help with the prototype manufacturing and measurements.

References

[1] *5G Spectrum, Public Policy Position*, Huawei, Shenzhen, China, 2020.
[2] M. Stanley, Y. Huang, H. Wang, H. Zhou, Z. Tian, and Q. Xu, "A novel reconfigurable metal rim integrated open slot antenna for octa-band smartphone applications," *IEEE Trans. Antennas Propag.*, vol. 65, no. 7, pp. 3352–3363, Jul. 2017.
[3] Z.-Q. Xu, Y. Sun, Q.-Q. Zhou, Y.-L. Ban, Y.-X. Li, and S. S. Ang, "Reconfigurable MIMO antenna for integrated-metal-rimmed smartphone applications," *IEEE Access*, vol. 5, pp. 21223–21228, 2017.
[4] Y.-H. Zhang, S.-R. Yang, Y.-L. Ban, Y.-F. Qiang, J. Guo, and Z.-F. Yu, "Four-feed reconfigurable MIMO antenna for metal-frame smartphone applications," *IET Microw., Antennas Propag.*, vol. 12, no. 9, pp. 1477–1482, Jul. 2018.
[5] L.-W. Zhang, Y.-L. Ban, C.-Y.-D. Sim, J. Guo, and Z.-F. Yu, "Parallel dual-loop antenna for WWAN/LTE metal-rimmed smartphone," *IEEE Trans. Antennas Propag.*, vol. 66, no. 3, pp. 1217–1226, Mar. 2018.
[6] J. Choi, W. Hwang, C. You, B. Jung, and W. Hong, "Four-element reconfigurable coupled loop MIMO antenna featuring LTE full-band operation for metallic-rimmed smartphone," *IEEE Trans. Antennas Propag.*, vol. 67, no. 1, pp. 99–107, Jan. 2019.
[7] J. Y. Deng, J. Yao, D. Q. Sun, and L. X. Guo, "Ten-element MIMO antenna for 5G terminals," *Microw. Opt. Technol. Lett.*, vol. 60, pp. 3045–3049, Dec. 2018.
[8] Y. Li, C.-Y.-D. Sim, Y. Luo, and G. Yang, "12-Port 5G massive MIMO antenna array in Sub-6GHz mobile handset for LTE bands 42/43/46 applications," *IEEE Access*, vol. 6, pp. 344–354, Oct. 2018.
[9] K.-L. Wong, C.-Y. Tsai, and J.-Y. Lu, "Two asymmetrically mirrored gap-coupled loop antennas as a compact building block for eight-antenna MIMO array in the future smartphone," *IEEE Trans. Antennas Propag.*, vol. 65, no. 4, pp. 1765–1778, Apr. 2017.
[10] L. Chang, Y. Yu, K. Wei, and H. Wang, "Polarization-orthogonal co-frequency dual antenna pair suitable for 5G MIMO smartphone with metallic bezels," *IEEE Trans. Antennas Propag.*, vol. 67, no. 8, pp. 5212–5220, Aug. 2019.
[11] A. Zhao and Z. Ren, "Wideband MIMO antenna systems based on coupled-loop antenna for 5G N77/N78/N79 applications in mobile terminals," *IEEE Access*, vol. 7, pp. 93761–93771, 2019.
[12] A. Zhao and Z. Ren, "Size reduction of self-isolated MIMO antenna system for 5G mobile phone applications," *IEEE Antennas Wireless Propag. Lett.*, vol. 18, no. 1, pp. 152–156, Jan. 2019.
[13] Z. Ren, A. Zhao, and S. Wu, "MIMO antenna with compact decoupled antenna pairs for 5G mobile terminals," *IEEE Antennas Wireless Propag. Lett.*, vol. 18, no. 7, pp. 1367–1371, Jul. 2019.

[14] Z. Ren and A. Zhao, "Dual-band MIMO antenna with compact self-decoupled antenna pairs for 5G mobile applications," *IEEE Access*, vol. 7, pp. 82288–82296, 2019.
[15] L. Sun, Y. Li, Z. Zhang, and Z. Feng, "Wideband 5G MIMO antenna with integrated orthogonal-mode dual-antenna pairs for metal-rimmed smartphones," *IEEE Trans. Antennas Propag.*, vol. 68, no. 4, pp. 2494–2503, Apr. 2020.
[16] D. Q. Liu, H. J. Luo, M. Zhang, H. L. Wen, B. Wang, and J. Wang, "An extremely low-profile wideband MIMO antenna for 5G smartphones," *IEEE Trans. Antennas Propag.*, vol. 67, no. 9, pp. 5772–5780, Sep. 2019.
[17] I. R. R. Barani, K.-L. Wong, Y. Zhang, and W. Li, "Low-profile wideband conjoined open-slot antennas fed by grounded coplanar waveguides for 4×4 5G MIMO operation," *IEEE Trans. Antennas Propag.*, vol. 68, no. 4, pp. 2646–2657, Apr. 2020.
[18] N. Liu, S. Gao, L. Zhu, L. Ji, L. Yang, and H. Zheng, "Low-profile microstrip patch antenna with simultaneous enhanced bandwidth, beamwidth, and cross-polarisation under dual resonance," *IET Microw., Antennas Propag.*, vol. 14, no. 5, pp. 360–365, 2020.
[19] R. Jian, Y. Chen, and T. Chen, "A low-profile wideband PIFA based on radiation of multiresonant modes," *IEEE Antennas Wireless Propag. Lett.*, vol. 19, no. 4, pp. 685–689, Apr. 2020.
[20] B. Cheng, Z. Du, and D. Huang, "A differentially fed broadband multi-mode microstrip antenna," *IEEE IEEE Antennas Wireless Propag. Lett.*, vol. 19, no. 5, pp. 1–5, May 2020.
[21] N.-W. Liu, M.-J. Sun, L. Zhu, D. Xie, and G. Fu, "A low-profile printed cavity antenna with simultaneous bandwidth and radiation pattern improvement," *IEEE Antennas Wireless Propag. Lett.*, vol. 18, no. 10, pp. 2125–2129, Oct. 2019.
[22] J. Singh, R. Stephan, and M. A. Hein, "Low-profile wideband differentially fed di-patch antenna closely above metallic ground," *IEEE Antennas Wireless Propag. Lett.*, vol. 18, no. 5, pp. 976–980, May 2019.
[23] N. Liu, X. Chen, L. Zhu, X. Chen, G. Fu, and Y. Liu, "Low-profile triple-band microstrip antenna via sharing a single multi-mode patch resonator," *IET Microw., Antennas Propag.*, vol. 13, no. 10, pp. 1580–1585, Aug. 2019.
[24] Q. Liu, L. Zhu, J. Wang, and W. Wu, "Wideband low-profile differential-fed patch antennas with an embedded SIW cavity under dual-mode resonance," *IEEE Trans. Antennas Propag.*, vol. 67, no. 6, pp. 4235–4240, Jun. 2019.
[25] D. Tayli and M. Gustafsson, "Physical bounds for antennas above a ground plane," *IEEE IEEE Antennas Wireless Propag. Lett.*, vol. 15, pp. 1281–1284, 2016.
[26] M. Gustafsson, M. Capek, and K. Schab, "Tradeoff between antenna efficiency and Q-factor," *IEEE Trans. Antennas Propag.*, vol. 67, no. 4, pp. 2482–2493, Apr. 2019.
[27] C.-Z. Han, G.-L. Huang, T. Yuan, W. Hong, and C.-Y.-D. Sim, "A frequency-reconfigurable tuner-loaded coupled-fed frame-antenna for all-metal-shell handsets," *IEEE Access*, vol. 6, pp. 64041–64049, 2018.
[28] Q. Chen *et al.*, "Single ring slot-based antennas for metal-rimmed 4G/5G smartphones," *IEEE Trans. Antennas Propag.*, vol. 67, no. 3, pp. 1476–1487, Mar. 2019.
[29] S. M. Asif, M. R. Anbiyaei, K. L. Ford, T. O'Farrell, and R. J. Langley, "Low-profile independently- and concurrently-tunable quad-band antenna for single chain sub-6 GHz 5G new radio applications," *IEEE Access*, vol. 7, pp. 183770–183782, 2019.
[30] H. F. Abutarboush *et al.*, "A reconfigurable wideband and multiband antenna using dual-patch elements for compact wireless devices," *IEEE Trans. Antennas Propag.*, vol. 60, no. 1, pp. 36–43, Jan. 2012.
[31] S. M. Asif, A. Iftikhar, S. M. Khan, M. Usman, and B. D. Braaten, "An E-shaped microstrip patch antenna for reconfigurable dual-band operation," *Microw. Opt. Technol. Lett.*, vol. 58, no. 6, pp. 1485–1490, Jun. 2016.
[32] H. Wang *et al.*, "Small-size reconfigurable loop antenna for mobile phone applications," *IEEE Access*, vol. 4, pp. 5179–5186, 2016.
[33] W.-W. Lee and B. Jang, "A tunable MIMO antenna with dual-port structure for mobile phones," *IEEE Access*, vol. 7, pp. 34113–34120, 2019.
[34] C.-Z. Han *et al.*, "A frequency-reconfigurable antenna with 1-mm nonground portion for metal-frame and full-display screen handset applications using mode control method," *IEEE Access*, vol. 7, pp. 48037–48045, 2019.
[35] Y. Kabiri, P. Gardner, and C. Constantinou, "A novel approach for wideband tunable electrically small antennas," in *Proc. 8th Eur. Conf. Antennas Propag. (EuCAP)*, Apr. 2014, pp. 3633–3637.
[36] Y. Kabiri, P. Gardner, and C. Constantinou, "Injection matched approach for wideband tunable electrically small antennas," *IET Microw., Antennas Propag.*, vol. 8, no. 11, pp. 878–886, Aug. 2014.
[37] J.-M. Hannula, J. Holopainen, and V. Viikari, "Concept for frequency-reconfigurable antenna based on distributed transceivers," *IEEE Antennas Wireless Propag. Lett.*, vol. 16, pp. 764–767, 2017.
[38] J.-M. Hannula, T. Saarinen, J. Holopainen, and V. Viikari, "Frequency reconfigurable multiband handset antenna based on a multichannel transceiver," *IEEE Trans. Antennas Propag.*, vol. 65, no. 9, pp. 4452–4460, Sep. 2017.
[39] J. Hannula, T. O. Saarinen, A. Lehtovuori, J. Holopainen, and V. Viikari, "Tunable eight-element MIMO antenna based on the antenna cluster concept," *IET Microw., Antennas Propag.*, vol. 13, no. 7, pp. 959–965, Jun. 2019.
[40] J.-M. Hannula, A. Lehtovuori, R. Luomaniemi, T. O. Saarinen, and V. Viikari, "Beneficial interaction of coupling and mismatch in a two-antenna system," in *Proc. 13th Eur. Conf. Antennas Propag. (EuCAP)*, Mar. 2019, pp. 1–4.
[41] R. Luomaniemi, P. Yla-Oijala, A. Lehtovuori, and V. Viikari, "Designing hand-immune handset antennas with adaptive excitation and characteristic modes," *IEEE Trans. Antennas Propag.*, vol. 69, no. 7, pp. 3829–3839, Jul. 2021, doi: 10.1109/TAP.2020.3044640.
[42] M. Manteghi and Y. Rahmat-Samii, "Multiport characteristics of a wide-band cavity backed annular patch antenna for multipolarization operations," *IEEE Trans. Antennas Propag.*, vol. 53, no. 1, pp. 466–474, Jan. 2005.
[43] R. Tian, B. K. Lau, and Z. Ying, "Multiplexing efficiency of MIMO antennas," *IEEE Antennas Wireless Propag. Lett.*, vol. 10, pp. 183–186, 2011.
[44] R. Luomaniemi, A. Salmi, A. Lehtovuori, and V. Viikari, "Reducing user effect on mobile antenna systems with antenna cluster technique," in *Proc. 14th Eur. Conf. Antennas Propag. (EuCAP)*, Mar. 2020, pp. 1–4.
[45] Y. H. Chen, K.-L. Wong, and W. Y. Li, "4×4 MIMO performance of two conjoined dual wideband antennas including the feedline effects for 5G smartphones," in *Proc. IEEE Asia–Pacific Microw. Conf. (APMC)*, Dec. 2019, pp. 1488–1490.

Rasmus Luomaniemi (Graduate Student Member, IEEE) was born in Salo, Finland, in 1994. He received the B.Sc. (Tech.) and M.Sc. (Tech.) degrees (Hons.) in electrical engineering from Aalto University, Espoo, Finland, in 2016 and 2018, respectively, where he is currently pursuing the D.Sc. (Tech.) degree.

Since 2014, he has been with the Department of Electronics and Nanoengineering, School of Electrical Engineering, Aalto University. His current research interests include multiple-input–multiple-output MIMO antennas for mobile devices and multiport antennas.

Mr. Luomaniemi was a recipient of the Second Prize in the IEEE AP-S Student Design Contest as a part of the Team Aalto ELEC in 2016.

Anu Lehtovuori received the M.Sc. (Tech.) and Lic.Sc. (Tech.) degrees from the Helsinki University of Technology, Espoo, Finland, in 2000 and 2003, respectively, and the D.Sc. (Tech.) degree from Aalto University, Espoo, in 2015, all in electrical engineering.

She is currently a University Lecturer in circuit theory with the School of Electrical Engineering, Aalto University. Her current research interests include electrically small antennas, multiport antennas, and design of antennas for mobile devices.

Janne Ilvonen was born in Helsinki, Finland, in 1976. He received the M.Sc. and Lic.Sc. degrees (Hons.) and the D.Sc. (Tech.) degree in electrical engineering from Aalto University, Espoo, Finland, in 2009, 2012, and 2014, respectively.

From 2015 to 2016, he was a Senior Antenna Engineer with Microsoft Mobile, Finland, where he was developing antenna concepts for Microsoft's future flagship handsets. Since 2016, he has been with Huawei Technologies Finland, Helsinki, as a Principal Antenna Engineer. His current research interest includes sub-6 GHz and mm-Wave 5G handset antennas.

Alexander Khripkov (Member, IEEE) received the B.S. degree in radio engineering and the Ph.D. degree in antennas and microwave devices from the Southern Federal University of Russia, Rostov-on-Don, Russia, in 2002 and 2007, respectively.

From 2007 to 2012, he was a Researcher with the Department of Ultrawide Band Sensors for Medical Applications, Industrial Technology Research Institute, Taiwan. From 2012 to 2016, he was a Group Leader of the Electromagnetic Solutions Group, Samsung R&D Institute, Moscow, Russia. He is currently a Principal Antenna Engineer with the Terminal Antenna and RF Laboratory, Huawei Technologies Finland, Helsinki, Finland. He has authored or coauthored about 30 articles in peer-reviewed journals and conference proceedings, and holds eight granted U.S. patents and about 20 granted patents in other countries. His current research interests include microwave/millimeter-wave antennas and circuits, millimeter-wave systems, terminal antennas, reconfigurable antenna arrays, and metamaterial-inspired structures.

Dr. Khripkov was a recipient of over ten industrial awards. He serves as a Reviewer for more than 20 journals in the IEEE Antennas and Propagation Society and the *IET Communications*.

Ville Viikari (Senior Member, IEEE) was born in Espoo, Finland, in 1979. He received the Master of Science (Tech.) and Doctor of Science (Tech.) (Hons.) degrees in electrical engineering from Helsinki University of Technology (TKK), Espoo, in 2004 and 2007, respectively.

From 2001 to 2007, he was with the Radio Laboratory, TKK, where he studied antenna measurement techniques at submillimeter wavelengths and antenna pattern correction techniques. From 2007 to 2012, he was a Research Scientist and Senior Scientist with the VTT Technical Research Center, Espoo, where his research included wireless sensors, RFID, radar applications, MEMS, and microwave sensors. He is currently an Associate Professor and the Deputy Head of the department, School of Electrical Engineering, Aalto University, Espoo. His current research interests include antennas for mobile networks, RF-powered devices, and antenna measurement techniques.

Dr. Viikari was a recipient of the Young Researcher Award of the year 2014 presented by the Finnish Foundation for Technology Promotion, the IEEE Sensors Council 2010 Early Career Gold Award, the 2008 Young Scientist Award of the URSI XXXI Finnish Convention on Radio Science, Espoo, and the Best Student Paper Award of the Annual Symposium of the Antenna Measurement Techniques Association, Newport, RI, USA, from October 30 to November 4, 2005. He has served as the Chair for the Technical Program Committee of the ESA Workshop on Millimeter-Wave Technology and Applications and the Global Symposium on Millimeter Waves (GSMM) in 2011 and 2016, Espoo.